We are IntechOpen,
the world's leading publisher of Open Access books
Built by scientists, for scientists

5,300
Open access books available

130,000
International authors and editors

155M
Downloads

154
Countries delivered to

Our authors are among the

TOP 1%
most cited scientists

12.2%
Contributors from top 500 universities

BOOK CITATION INDEX
CLARIVATE ANALYTICS
INDEXED

WEB OF SCIENCE™

Selection of our books indexed in the Book Citation Index
in Web of Science™ Core Collection (BKCI)

Interested in publishing with us?
Contact book.department@intechopen.com

Numbers displayed above are based on latest data collected.
For more information visit www.intechopen.com

Analysis of Quiet Zones in Diffuse Fields

Wen-Kung Tseng
National Changhua University of Education
Taiwan, R.O.C.

1. Introduction

Generally speaking, the aim of active noise control systems is to control noise at a dominant frequency range and at a specified region in space. Conventional approaches to active noise control are to cancel the noise at one point in space over a certain frequency range or at many points in space for a single-tone disturbance [Ross, 1980; Joseph, 1990; Nelson & Elliott, 1992]. Cancelling the noise at one point would produce a limited zone of quiet with no control over its shape. Although cancelling the noise at many points could produce larger zones of quiet, the optimal spacing between cancellation points varies with frequency [Miyoshi et al., 1994; Guo et al., 1997].

Previous work on active control of diffuse fields investigated the performance of pressure attenuation for single-tone diffuse field only which was produced by single frequency [Ross, 1980; Joseph, 1990; Tseng, 1999, 2000]. Recent work on broad-band diffuse fields only concentrated on analysis of auto-correlation and cross-correlation of sound pressure [Rafaely, 2000, 2001; Chun et al., 2003]. However there is only some work related to active control of broad-band diffuse fields [Tseng, 2009]. Therefore this chapter will analyze the quiet zones in pure tone and broad-band diffuse fields using ∞-norm pressure minimization.

Moreover a constrained minimization of acoustic pressure is introduced, to achieve a better control of acoustic pressure in space or both frequency and space. The chapter is organized as follows. First, the mathematical model of pure tone and broad-band diffuse fields is derived. Second, the theory of active control for pure tone and broad-band diffuse fields is introduced. Next, simulation results of quiet zones in pure tone and broad-band diffuse fields are presented. Then, preliminary experiments are described. Finally the conclusions are made.

2. The wave model of pure tone and broad-band diffuse sound fields

Garcia-Bonito used the wave model for a pure tone diffuse field, which is comprised of large number of propagating waves arriving from various directions [Garcia et al., 1997]. However, a complete mathematical derivation of this model, which was taken from Jacobson [Jacobsen, 1979], was not found and the wave model of broadband diffuse sound fields has not been derived. For completeness, this mathematical derivation for pure tone and broadband diffuse fields is given below.

When a source produces sound in an enclosure in a room, the sound field is composed of two fields. One is the sound field radiated directly from the source called the direct sound

field. The other is reflection of sound waves from surfaces of the room, which contributes to the overall sound field, this contribution being known as the reverberant field. Therefore at any point in the room, the sound field is a function of direct and reverberant sound fields. The sound field in a reverberant space can be divided into two frequency ranges. In the low frequency range, the room response is dominated by standing waves at certain frequencies. In the high frequency range, the resonances become so numerous that they are difficult to distinguish from one another. For excitation frequencies greater than the Schroeder frequency, for which M (ω) = 3, where M(ω) is the modal overlap [Garcia et al., 1997], the resulting sound field is essentially diffuse and may be described in statistical terms or in terms of its average properties. The diffuse sound field model can be derived as follows.

In the model described below, the diffuse field is comprised of many propagating waves with random phases, arriving from uniformly distributed directions. Although the waves occupy a three-dimensional space, the quiet zone analysis is performed, for simplicity, over a two-dimensional area. Consider a single incident plane wave travelling along line r with its wave front parallel to lines *A* and *B* as shown in Figure 1. We assume that the plane wave has some phase when approaching line *A*, and has some phase shift due to the time delay when approaching line *B* both on the *x-y* plane. We next find the phase of the plane wave at (x_0, y_0) on line *B*. We now consider the plane perpendicular to lines *A* and *B* and parallel to line *r*, as illustrated in Figure 2. This incident plane wave has phase shift when approaching point (x_0, y_0) on line *B*. The pressure at this point can therefore be expressed as

$$P(x_0, y_0, k) = (a+jb) \exp(-jkd) \tag{1}$$

where *a+jb* account for the amplitude and phase of this incident plane wave when approaching line *A*, *k* is the wave number and *d* is the additional distance travelled by the plane wave when approaching point (x_0, y_0) on line *B* as shown in Figure 2.
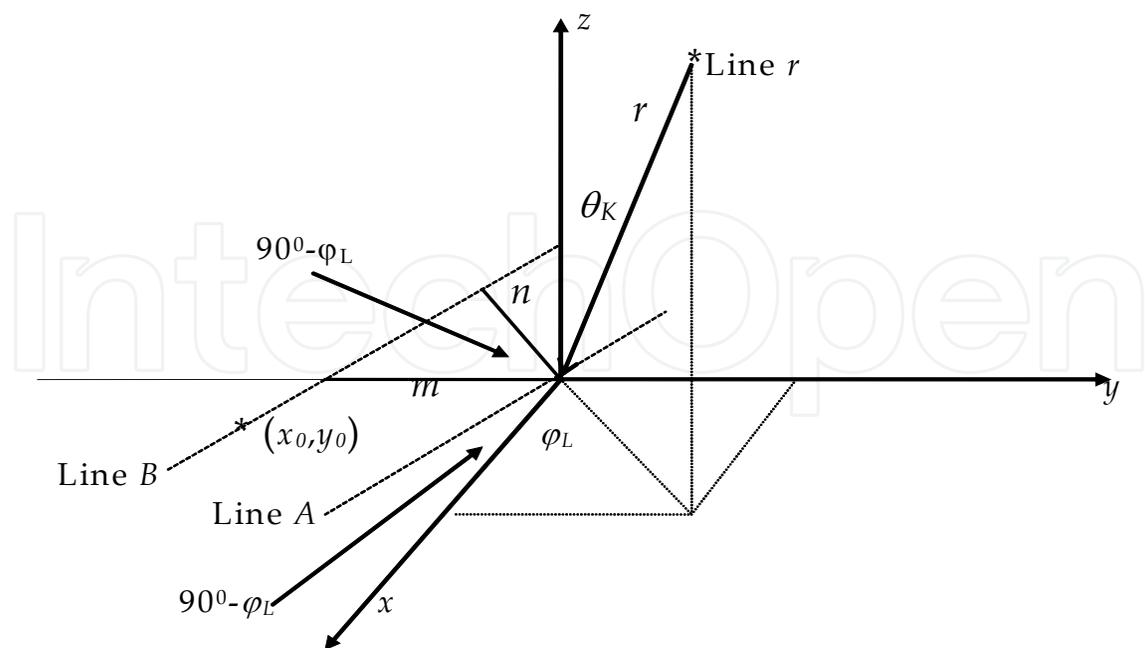

Fig. 1. Definition of spherical co-ordinates *r*, θ, φ for an incident plane wave travelling alone line *r* direction.
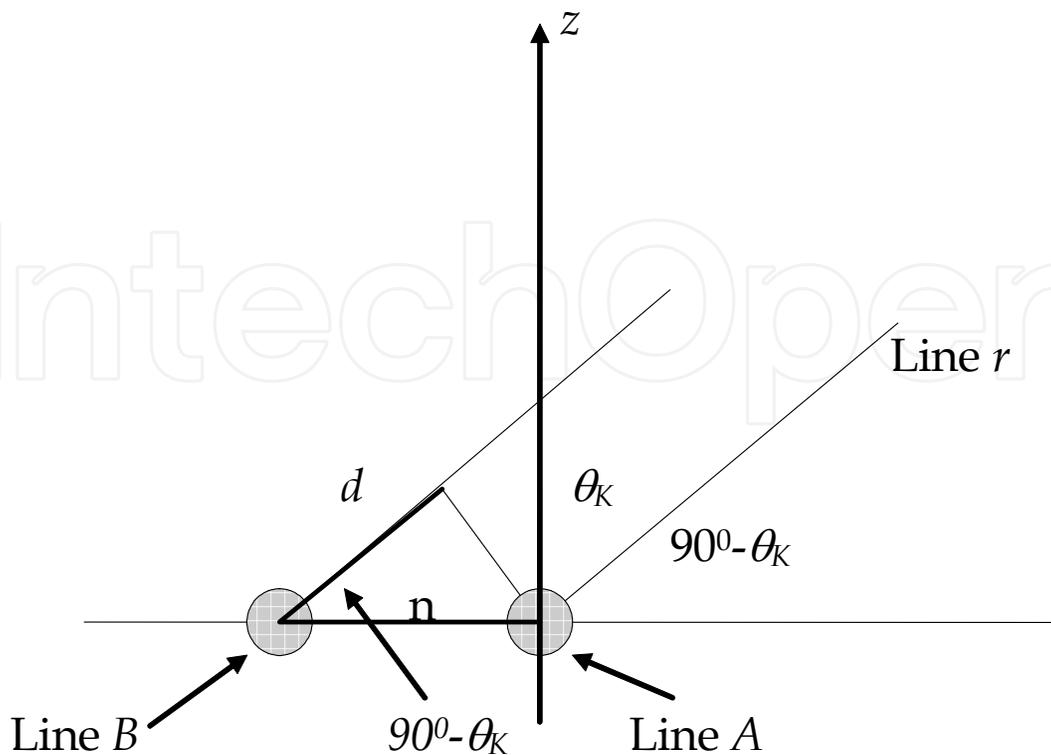
Fig. 2. The plane perpendicular to lines *A* and *B* and parallel to line *r*.

The equation of line *A* on the *x-y* plane can be written as

$$y = -x \tan(90^0 - \varphi_L) = -x \cot\varphi_L \tag{2}$$

The equation of line *B* on *x-y* plane can also be written as

$$y = -x \tan(90^0 - \varphi_L) + m = -x \cot\varphi_L - m \tag{3}$$

where *m* is the distance between lines *A* and *B* on the *y*-axis.
Substituting (x_0, y_0) into Equation (3) gives

$$m = -y_0 - x_0 \cot\varphi_L \tag{4}$$

The distance *n* between lines *A* and *B* as in Figure 1 can now be calculated as

$$n = m \cos(90^0 - \varphi_L) = m \sin\varphi_L \tag{5}$$

Substituting equation (4) into equation (5), the distance *n* becomes

$$n = -y_0 \sin\varphi_L - x_0 \cos\varphi_L \tag{6}$$

The distance *d* in figure 2 can now be calculated as

$$d = n \cos(90^0 - \theta_K) = n \sin\theta_K \tag{7}$$

Equation (6) can be substituted into equation (7) and the distance *d* becomes

$$d = -y_0 \sin\theta_K \sin\varphi_L - x_0 \sin\theta_K \cos\varphi_L \tag{8}$$

Therefore equation (1) can be written as

$$P(x_0,y_0, k) = (a+jb) \exp(jk(y_0 \sin \theta_K \sin \varphi_L + x_0 \sin \theta_K \cos \varphi_L)) \tag{9}$$

In our study we chose 72 such incident plane waves together with random amplitudes and phases to generate an approximation of a diffuse sound field in order to coincide with that in previous work. Thus the diffuse sound field was generated by adding together the contributions of 12 plane waves in the azimuthal directions (corresponding to azimuthal angles $\varphi_L = L \times 30^0$, $L=1,2,3, \ldots , 12$) for each of six vertical incident directions (corresponding to vertical angles $\theta_K = K \times 30^0$ for $K = 1, 2, 3, \ldots , 6$). The net pressure in the point (x_0,y_0) on the x-y plane due to the superposition of these 72 plane waves is then calculated from the expression

$$P_p(x_0,y_0, k) = \sum_{K=1}^{K\max} \sum_{L=1}^{L\max} (a_{KL} +jb_{KL}) \sin\theta_K \exp(jk(x_0 sin\theta_K cos\varphi_L + y_0 sin\theta_K sin\varphi_L)) \tag{10}$$

in which both the real and imaginary parts of the complex pressure are randomly distributed. The values of a_{KL} and b_{KL} are chosen from a random population with Gaussian distribution $N(0,1)$ and the multiplicative factor $\sin\theta_K$ is included to ensure that, on average, the energy associated with the incident waves was uniform from all directions. Each set of 12 azimuthal plane waves arriving from a different vertical direction θ_K , is distributed over a length of $2\pi r \sin\theta_K$, which is the circumference of the sphere defined by (r,φ,θ) for θ_K. This results in higher density of waves for smaller θ_K , and thus more energy associated with small θ_K . To ensure uniform energy distribution, the amplitude of the waves is multiplied by $\sin\theta_K$, thus making the waves coming from the ''dense'' direction, lower in amplitude. Substituting $k=\dfrac{2\pi}{c}f$ into equation (10) gives

$$P_p(x_0,y_0,f) = \sum_{K=1}^{K\max} \sum_{L=1}^{L\max} (a_{KL} + jb_{KL})\sin\theta_K \exp(j\frac{2\pi}{c}f(x_0 \sin\theta_K \cos\varphi_L + y_0 \sin\theta_K \sin\varphi_L)) \tag{11}$$

Where f is frequency and c the speed of sound. Equation (11) is the wave model of the pure tone diffuse field since only the single frequency plane wave arriving from uniformly distributed directions is considered. If the diffuse field is broad-band within the frequency range of fl and fh, then the wave model of the broad-band diffuse field P_{pb} can be expressed as

$$P_{pb}(x_0,y_0,fl-fh) = \sum_{f=fl}^{fh} \sum_{K=1}^{K\max} \sum_{L=1}^{L\max} (a_{KL} + jb_{KL})\sin\theta_K \exp(j\frac{2\pi}{c}f(x_0 \sin\theta_K \cos\varphi_L + y_0 \sin\theta_K \sin\varphi_L))$$

$$\tag{12}$$

Where fl-fh is the frequency range from fl to fh Hz. Equation (12) will be used for broad-band diffuse primary sound field in this work. Next we will describe the formulation of the control method, and their use in the design of quiet zones for pure tone and broad-band diffuse fields.

3. Theory of pressure minimization for pure tone and broad-band diffuse fields

In this section we present the theory of actively controlling pure tone and broad-band diffuse fields. The basic idea is to minimize acoustic pressure over an area in space for pure tone diffuse primary fields or in both space and frequency for broadband diffuse primary fields. Figure 3 illustrates the configuration of acoustic pressure minimization over space and frequency. In this work, the case of two-dimensional space is considered for pure tone diffuse fields derived in equation (11) and the case of a one-dimensional space and frequency is considered for broad-band diffuse primary fields derived in equation (12). The secondary sources are located at the (0.05m, 0) and (-0.05m, 0) point. A microphone can be placed at the desired zone of quiet or other locations close to secondary monopoles. The secondary sources are driven by feedback controllers connected to the microphone. The microphone detects the signal of the primary field, which is then filtered through the controllers to drive the secondary sources. The signals from the secondary sources are then used to attenuate the diffuse primary disturbance at the pressure minimization region.

The x-axis in figure. 3 is a one-dimensional spatial axis, which could be extended in principle, to 2 or 3D. The desired zone of quiet can be defined on this axis where a good attenuation is required. The y-axis is the frequency axis where the control bandwidth could be defined. The acoustic disturbance is assumed to be significant at the control frequency bandwidth. The shadowed region is the pressure minimization region, i.e., the desired zone of quiet over space and frequency. The region to the right of the pressure minimization region is the far field of the secondary sources, with a small control effort, and thus a small effect of the active system on the overall pressure. The region to the left of the pressure minimization region is the near field of the secondary sources, which might result in the amplification of pressure at this region. To avoid significant pressure amplification a pressure amplification constraint should be included in the design process using a constrained optimization. The region above and below the pressure minimization region represents frequency outside the bandwidth. Due to the waterbed effect (Skogestad & Postlethwaite, 1996), a decrease in the disturbance at the control bandwidth will result in amplification outside the bandwidth. Therefore, pressure amplification outside the bandwidth must be constrained in the design process.

The feedback system used in this work is shown in figure 4 and is configured using the internal model control as shown in figure 5 (Morari & Zafiriou, 1989), where P_1 is plant 1, the response between the input to the first monopole and the output of the microphone, P_{1o} is the internal model of plant 1, P_2 is plant 2, the response between the input to the second monopole and the output of the microphone, P_{2o} is the internal model of plant 2, P_{s1} and P_{s2} are the secondary fields at the field point away from the first and second monopoles respectively, d is the disturbance, the broad-band diffuse field, at the microphone location, d_s is the disturbance at the field point away from the microphone, and e is the error signal. In this work, P_{1o} is assumed to be equal to P_1 and P_{2o} is equal to P_2. Therefore the feedback system turns to a feedforward system with $x=d$, where x is the input to the control filters W_1 and W_2.

It is also assumed that the secondary and primary fields in both space and frequency, are known, and although a microphone is used for the feedback signal, pressure elsewhere is assumed to be known and this knowledge is used in the minimization formulation. Although it is not always practical to have a good estimate of pressure far from the

microphone, this still can be achieved in some cases using virtual microphone techniques which provide a sufficiently accurate estimate of acoustic pressure far from the microphone (Garcia et al., 1997).
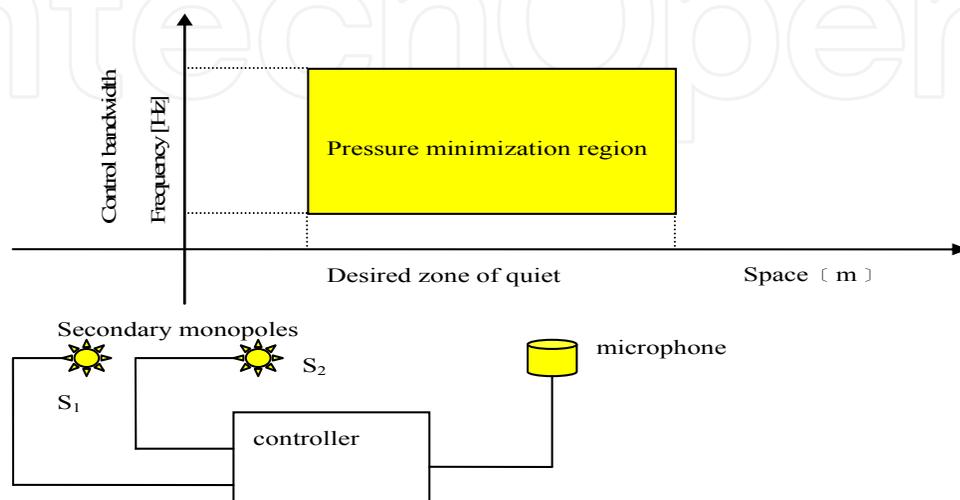

Fig. 3. Configuration of acoustic pressure minimization over space and frequency with a two-channel feedback system.
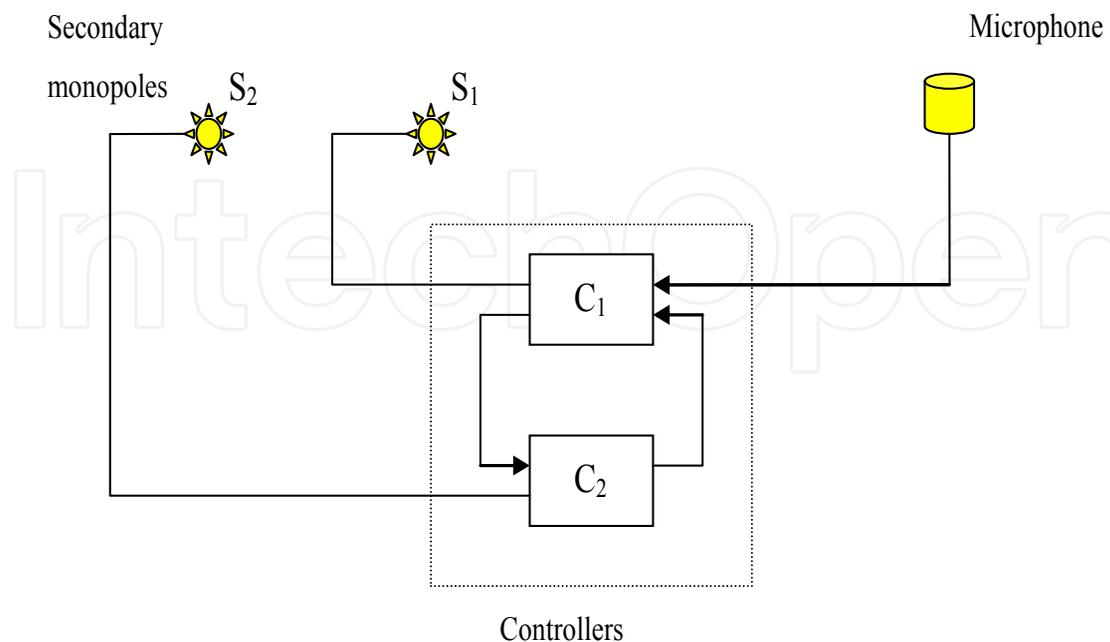

Fig. 4. Two-channel feedback control system used to control broad-band diffuse fields.
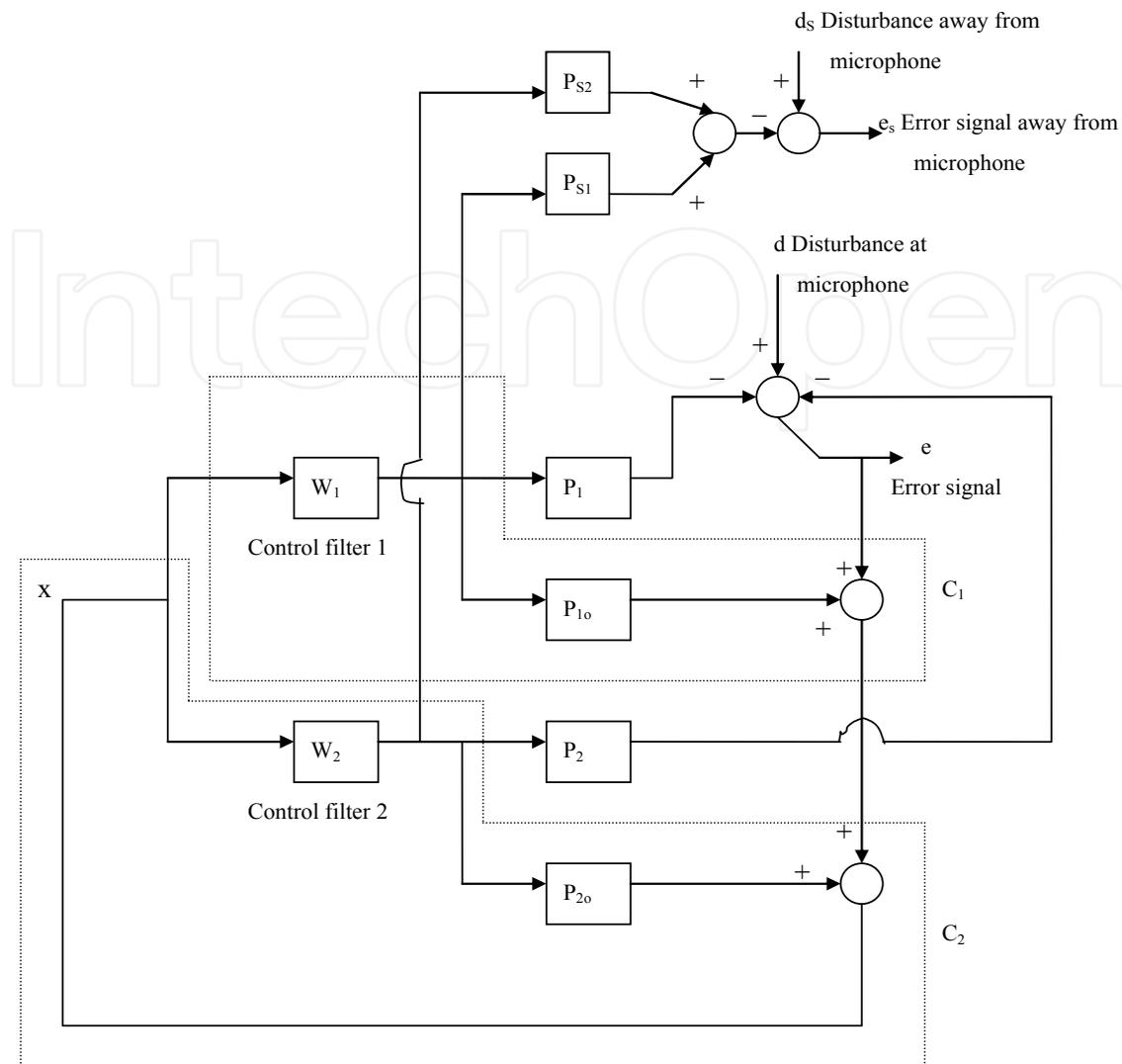
Fig. 5. Two-channel feedback control system with two internal model controllers.

The secondary fields at the field point away from the secondary monopoles could be written as (Miyoshi et al., 1994):

$$P_{s1}(r_1, f) = \frac{A_1}{r_1} e^{-j2\pi f r_1/c} \tag{13}$$

$$P_{s2}(r_2, f) = \frac{A_2}{r_2} e^{-j2\pi f r_2/c} \tag{14}$$

where r_1 and r_2 are the distances from the field point to the first and second monopoles, respectively, A_1 and A_2 are the amplitude constants, f is the frequency and c is the speed of sound.

The plant responses can be written as:

$$P_1(r_{1o}, f) = \frac{A_{1o}}{r_{1o}} e^{-j2\pi f r_{1o}/c} \tag{15}$$

$$P_2(r_{2o}, f) = \frac{A_{2o}}{r_{2o}} e^{-j2\pi f r_{2o}/c} \tag{16}$$

where r_{1o} and r_{2o} are the distances from the microphone to the first and second monopoles, A_{1o} and A_{2o} are the amplitude constants. The error signal could be expressed as:

$$
\begin{aligned}
e_s &= d_s - d_s W_1 P_{s1} - d_s W_2 P_{s2} \\
&= d_s(1 - W_1 P_{s1} - W_2 P_{s2}) \\
&= d_s(1 - W_1 \frac{A_1}{r_1} e^{-j2\pi f r_1/c} - W_2 \frac{A_2}{r_2} e^{-j2\pi f r_2/c})
\end{aligned}
\tag{17}
$$

The term $(1 - W_1 \frac{A_1}{r_1} e^{-j2\pi f r_1/c} - W_2 \frac{A_2}{r_2} e^{-j2\pi f r_2/c})$ is the sensitivity function [Franklin et al., 1994].

The disturbance in this work is the pure tone and broad-band diffuse fields, therefore equation (17) can also be expressed as:

$$e_s = P_p(1 - W_1 \frac{A_1}{r_1} e^{-j2\pi f r_1/c} - W_2 \frac{A_2}{r_2} e^{-j2\pi f r_2/c}) \qquad \text{for pure tone diffuse fields} \tag{18}$$

$$e_s = P_{pb}(1 - W_1 \frac{A_1}{r_1} e^{-j2\pi f r_1/c} - W_2 \frac{A_2}{r_2} e^{-j2\pi f r_2/c}) \qquad \text{for broad-band diffuse fields} \tag{19}$$

Where P_p is the pure tone diffuse primary field as shown in equation (11) and P_{pb} is the broad-band diffuse primary field as shown in equation (12).

The formulation of the cost function to be minimized can be written as.

$$J_\infty(r_1, r_2, f) = \left\| \sqrt{SP_p}(1 - W_1 \frac{A_1}{r_1} e^{-j2\pi f r_1/c} - W_2 \frac{A_2}{r_2} e^{-j2\pi f r_2/c}) \right\|_\infty \qquad \text{for pure tone diffuse fields} \tag{20}$$

$$J_\infty(r_1, r_2, f) = \left\| \sqrt{SP_{pb}}(1 - W_1 \frac{A_1}{r_1} e^{-j2\pi f r_1/c} - W_2 \frac{A_2}{r_2} e^{-j2\pi f r_2/c}) \right\|_\infty \qquad \text{for broad-band diffuse fields} \tag{21}$$

Where $\sqrt{SP_p}$ and $\sqrt{SP_{pb}}$ are the square root of the power spectral density of the pure tone and broad-band disturbance pressure at the field points respectively.

For a robust stability, the closed-loop of the feedback system must satisfy the following condition.

$$\left\| W_1 B_1 \frac{A_{1o}}{r_{1o}} e^{-j2\pi f r_{1o}/c} + W_2 B_2 \frac{A_{2o}}{r_{2o}} e^{-j2\pi f r_{2o}/c} \right\|_\infty < 1 \tag{22}$$

where B_1 and B_2 are the multiplicative plant uncertainty bounds for plants 1 and 2 and r_{1o} and r_{2o} are the distances from the microphone to the first and second monopoles, respectively. The terms $e^{-j2\pi f r_{1o}/c}$ and $e^{-j2\pi f r_{2o}/c}$, that are the plant responses, therefore, follow the robust stability condition, $\|WPB\|_\infty < 1$. For the amplification limit, a constraint could be added to the optimization process as follows.

$$\left\| (1 - W_1 \frac{A_1}{r_1} e^{-j2\pi f r_1/c} - W_2 \frac{A_2}{r_2} e^{-j2\pi f r_2/c}) D \right\|_\infty < 1 \tag{23}$$

where $1/D$ is the desired enhancement bound.

Therefore the overall design objective for the pure tone primary diffuse fields can now be written as:

$$min \quad \sigma$$

$$\left\| \sqrt{SP_p} (1 - W_1 \frac{A_1}{r_1} e^{-j2\pi f r_1/c} - W_2 \frac{A_2}{r_2} e^{-j2\pi f r_2/c}) \right\|_\infty < \sigma$$

$$subject\ to \quad \left\| W_1 B_1 \frac{A_{1o}}{r_{1o}} e^{-j2\pi f r_{1o}/c} + W_2 B_2 \frac{A_{2o}}{r_{2o}} e^{-j2\pi f r_{2o}/c} \right\|_\infty < 1 \tag{24}$$

$$\left\| (1 - W_1 \frac{A_1}{r_1} e^{-j2\pi f r_1/c} - W_2 \frac{A_2}{r_2} e^{-j2\pi f r_2/c}) D \right\|_\infty < 1$$

Also the overall design objective for the broad-band primary diffuse fields can now be written as:

$$min \quad \sigma$$

$$\left\| \sqrt{SP_{pb}} (1 - W_1 \frac{A_1}{r_1} e^{-j2\pi f r_1/c} - W_2 \frac{A_2}{r_2} e^{-j2\pi f r_2/c}) \right\|_\infty < \sigma$$

$$subject\ to \quad \left\| W_1 B_1 \frac{A_{1o}}{r_{1o}} e^{-j2\pi f r_{1o}/c} + W_2 B_2 \frac{A_{2o}}{r_{2o}} e^{-j2\pi f r_{2o}/c} \right\|_\infty < 1 \tag{25}$$

$$\left\| (1 - W_1 \frac{A_1}{r_1} e^{-j2\pi f r_1/c} - W_2 \frac{A_2}{r_2} e^{-j2\pi f r_2/c}) D \right\|_\infty < 1$$

Equation (24) can be reformulated by approximating r at discrete points only. The discrete space constrained optimization problem can now be written as:

$$min \quad \sigma$$

$$subject\ to \quad \left|\sqrt{SP_p}(1-W_1\frac{A_1}{r_1}e^{-j2\pi fr_1/c}-W_2\frac{A_2}{r_2}e^{-j2\pi fr_2/c})\right|<\sigma \quad for\ all\ r_1\ and\ r_2\ .$$

$$\left|W_1B_1\frac{A_{1o}}{r_{1o}}e^{-j2\pi fr_{1o}/c}+W_2B_2\frac{A_{2o}}{r_{2o}}e^{-j2\pi fr_{2o}/c}\right|<1 \quad for\ r_{1o}\ and\ r_{2o} \tag{26}$$

$$\left|(1-W_1\frac{A_1}{r_1}e^{-j2\pi fr_1/c}-W_2\frac{A_2}{r_2}e^{-j2\pi fr_2/c})D\right|<1 \quad for\ r_1\ and\ r_2\ .$$

Equation (25) can be reformulated by approximating f and r at discrete points only. The discrete frequency and space constrained optimization problem can now be written as:

$$min \quad \sigma$$

$$subject\ to \quad \left|\sqrt{SP_{pb}}(1-W_1\frac{A_1}{r_1}e^{-j2\pi fr_1/c}-W_2\frac{A_2}{r_2}e^{-j2\pi fr_2/c})\right|<\sigma \quad for\ all\ f,\ r_1\ and\ r_2\ .$$

$$\left|W_1B_1\frac{A_{1o}}{r_{1o}}e^{-j2\pi fr_{1o}/c}+W_2B_2\frac{A_{2o}}{r_{2o}}e^{-j2\pi fr_{2o}/c}\right|<1 \quad for\ all\ f,\ r_{1o}\ and\ r_{2o} \tag{27}$$

$$\left|(1-W_1\frac{A_1}{r_1}e^{-j2\pi fr_1/c}-W_2\frac{A_2}{r_2}e^{-j2\pi fr_2/c})D\right|<1 \quad for\ all\ f,\ r_1\ and\ r_2\ .$$

It should be noted that constraints on amplification and robust stability will be used in the simulations below. In the next section we will present the quiet zone analysis in pure tone and broad-band diffuse fields.

4. Quiet zone analysis in pure tone and broad-band diffuse fields

In this section the quiet zone analysis in pure tone and broad-band diffuse fields using two-channel and three-channel systems is investigated. The primary fields are pure tone and broad-band diffuse fields. In this work two and three monopoles are used as the secondary fields and a microphone is placed at the (0.1 m, 0) point, i.e., 10cm from the origin. The reason for choosing this configuration is because the previous study on pure tone and broad-band diffuse fields used the same configuration [Ross, 1980; Joseph, 1990; Tseng, 1999, 2000, 2009; Rafaely, 2000, 2001; Chun et al., 2003]. A series of examples are performed to analyze the quiet zones in pure tone and broadband diffuse fields. The theory described in previous sections is used for the simulations.

For the quiet zone simulations in the pure tone diffuse primary field two secondary monopoles are used to control the pure tone diffuse fields and zones of quiet for the two monopoles case are presented. Equation (26) is used to design the quiet zones. Figure 6 shows the 10 dB reduction contour line (solid curve) for two-channel system with two FIR filters having 64 coefficients with the robust constraint only using the ∞-norm strategy, minimizing the pressure over an area represented by a rectangular frame for 108Hz. The

two secondary monopoles located at (0.05, 0) and (-0.05, 0) are marked by '*'. The 10 dB amplification is also shown for the ∞-norm minimization strategy (dashed line). Figure 6 shows that ∞-norm strategy minimizing the pressure over an area produces a large zone enclosed by the 10 dB reduction contour. The reason for this is because the ∞-norm is to minimize the maximum pressure within the minimization area resulting in the optimal secondary field over the area. Figure 7 shows the same results for 216Hz. As can be seen from the figure the 10 dB quiet zone becomes smaller for 216Hz than that for 108Hz. This is due to the fact that the primary diffuse field becomes more complicated when the frequency is increased. Thus the primary diffuse field is more difficult to be controlled.
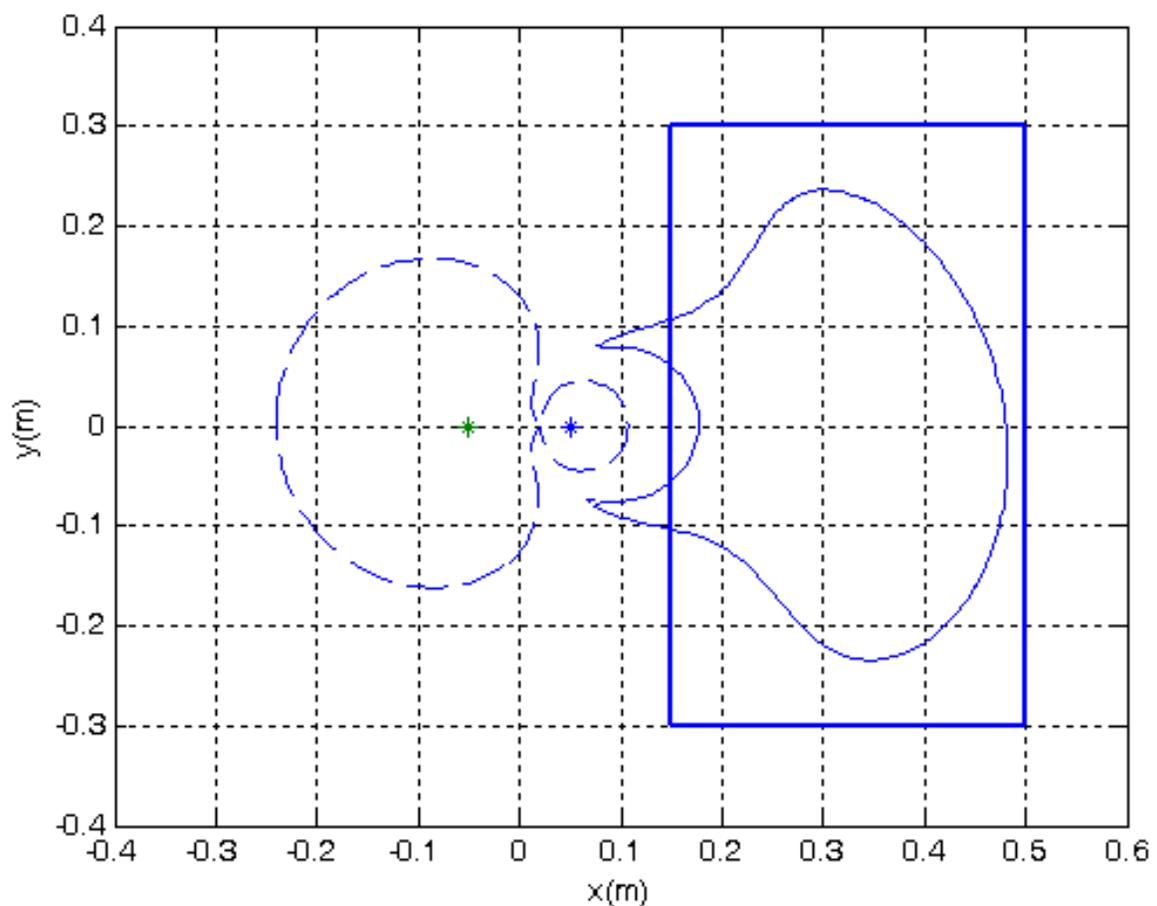
Fig. 6. The 10 dB reduction contour of the zones of quiet created by two secondary monopole sources located at positions (0.05, 0) and (-0.05, 0) for two-channel system with two FIR filters having 64 coefficients with the robust constraint only, minimizing the acoustic pressure at an area represented by a bold rectangular frame using ∞-norm minimization strategy (——), and the 10 dB increase in the primary field for 108Hz.
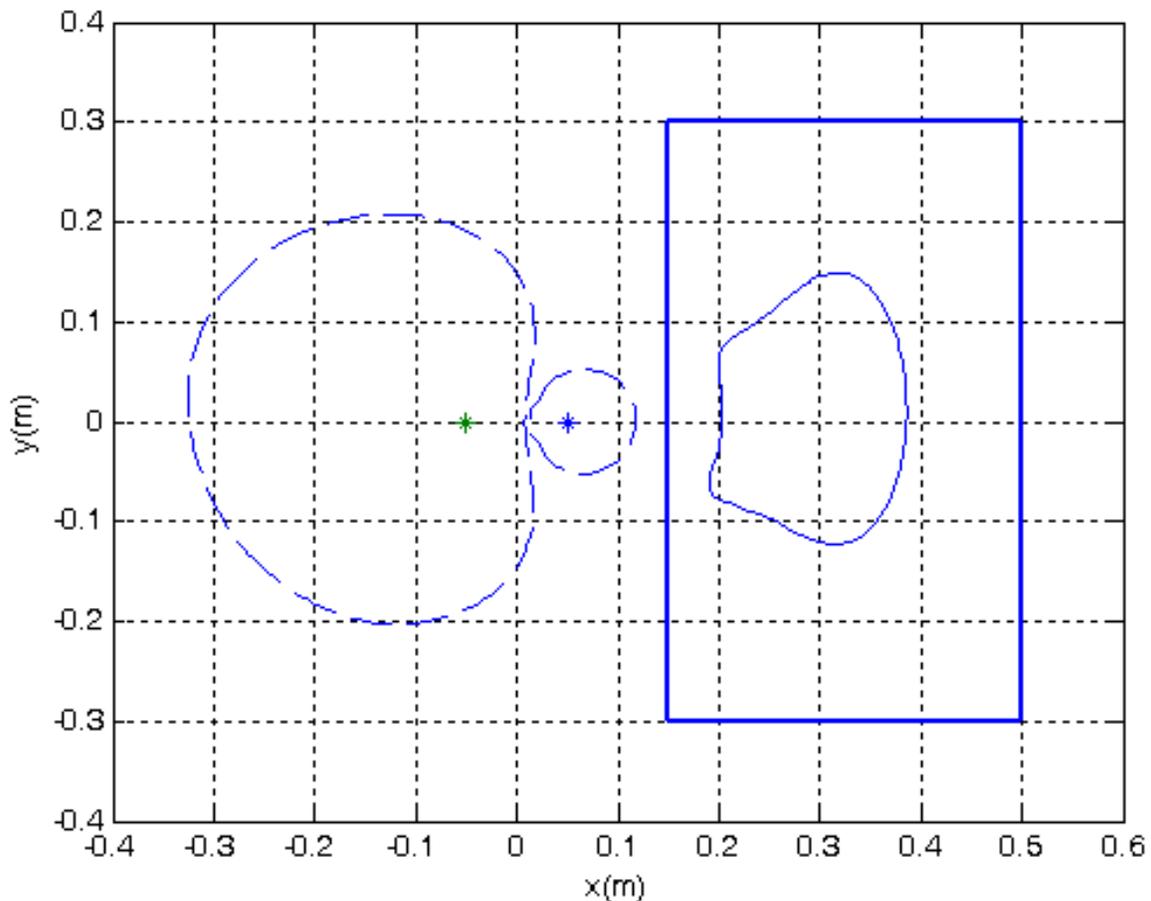
Fig. 7. The 10 dB reduction contour of the zones of quiet created by two secondary monopole sources located at positions (0.05, 0) and (-0.05, 0) for two-channel system with two FIR filters having 64 coefficients with the robust constraint only, minimizing the acoustic pressure at an area represented by a bold rectangular frame using ∞-norm minimization strategy (——), and the 10 dB increase in the primary field for 216Hz.

The zone of quiet created by introducing three secondary monopoles using ∞-norm minimization has also been explored. Figure 8 shows the 10 dB reductions in the pressure level (solid line) for ∞-norm minimization of the pressure in an area represented by the bold rectangular frame. The three secondary monopoles are located at (0, 0), (0.05, 0) and (-0.05, 0) represented by '*', and the 10 dB amplification in the acoustic pressure of the diffuse primary field is represented by a dashed line. Figure 8 shows that three secondary monopoles create a significantly larger zone of quiet than that in the two secondary monopoles case. However the size of the 10 dB amplification in the acoustic pressure away from the zone of quiet is also larger in this case. This shows that larger number of secondary sources provide better control over the secondary field, with the potential of producing larger zones of quiet at required locations.
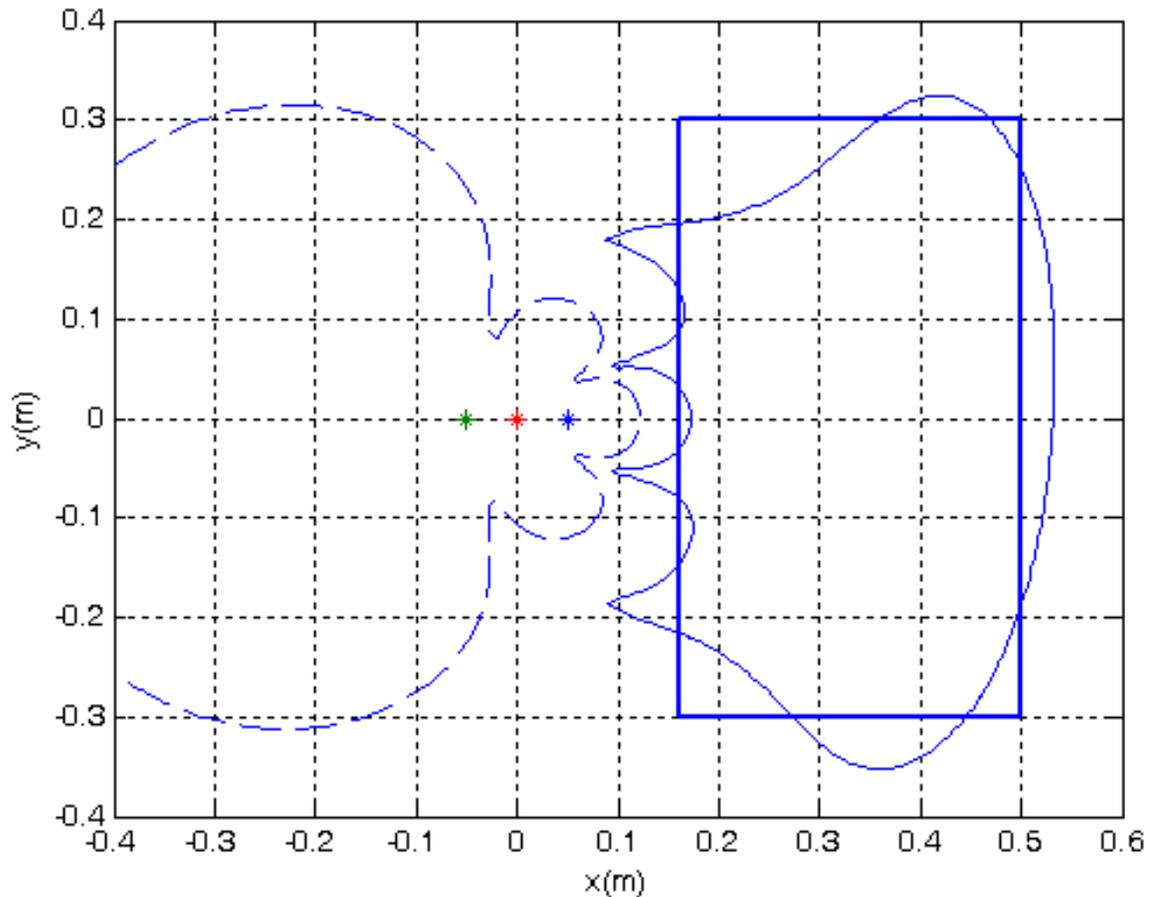
Fig. 8. The 10 dB reduction contour of the zones of quiet created by three secondary monopole sources located at positions (0.05, 0), (0, 0) and (-0.05, 0) for three-channel system with three FIR filters having 64 coefficients without constraints, minimizing the acoustic pressure at an area represented by a bold rectangular frame using ∞-norm minimization strategy (———), and the 10 dB increase in the primary field for 108Hz.

For quiet zone simulations in the broad-band diffuse primary field two secondary monopoles are used to control the broad-band diffuse fields. Equation (21) is used as the cost function to be minimized and equation (27) is used to design the quiet zones. The coefficients of the control filters with 64 coefficients were calculated using the function *fmincon()* in MATLAB. The attenuation contour over space and frequency for the two-channel system is shown in figure 9. The secondary monopoles are located at the (0.05 m, 0) and (-0.05 m, 0) points, and the minimization area is the region enclosed in the rectangle as shown in figure 9. From the figure we can observe that a high attenuation is achieved in the desired region. It can also be noted that the shape of the high-attenuation area is similar to that of the minimization region. This is because two monopoles could generate complicated secondary fields. Thus a good performance over the minimization region was obtained. A high amplification also appears at high-frequency regions and at the region close to the secondary monopoles. The attenuation contours on x-y plane at 400Hz and 600Hz are also shown in figures 10 (a) and (b). As can be seen from the figures the shape of the attenuation contour is shell-like.
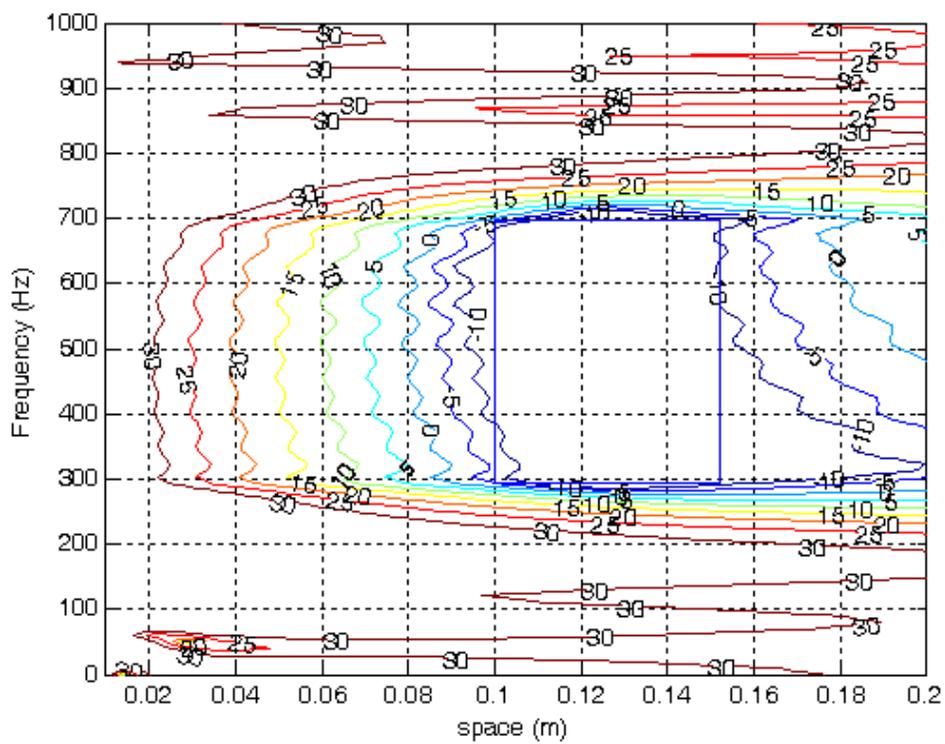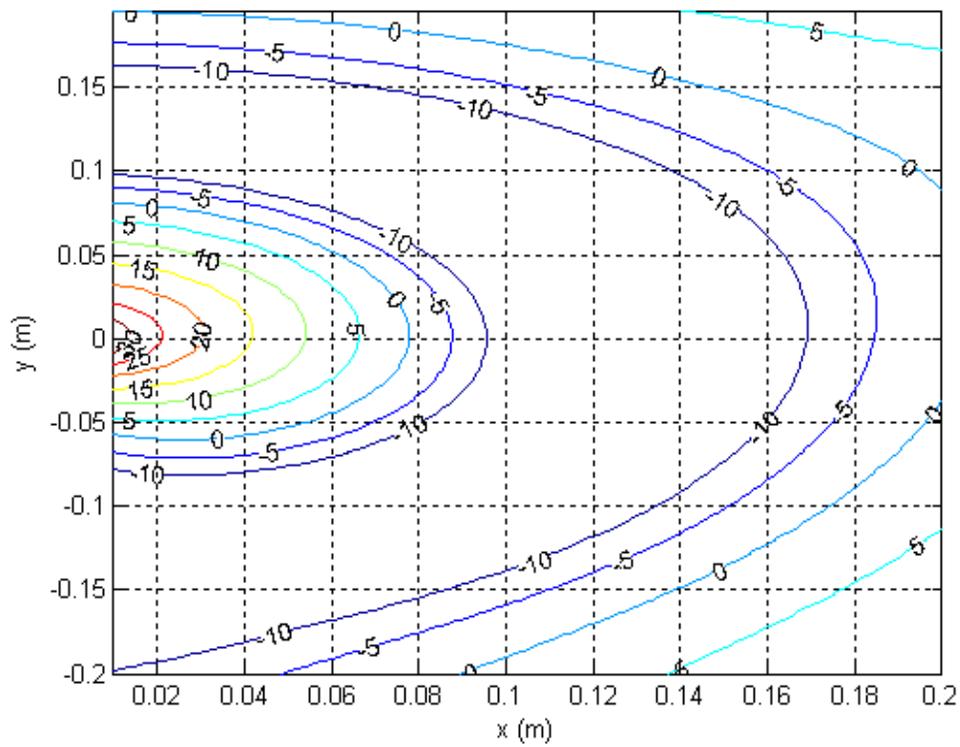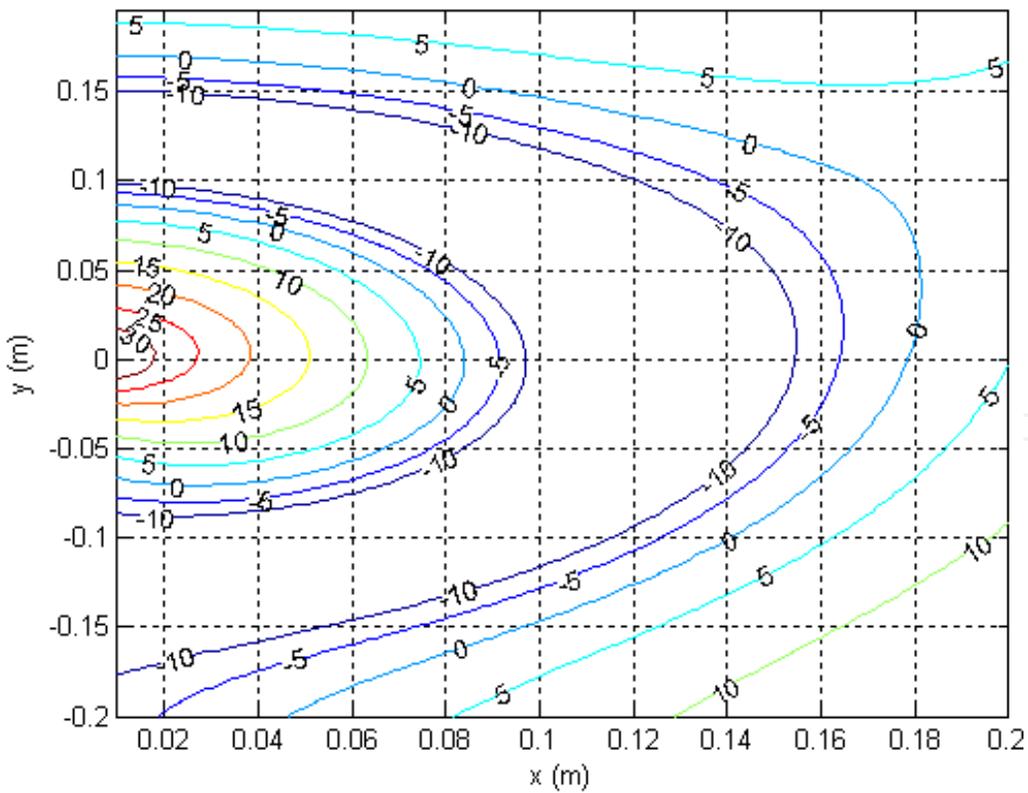
Fig. 9. Attenuation in decibels as a function of space and frequency for two-channel system with two FIR filters having 64 coefficients without constraints for broadband diffuse primary fields.

(a)

(b)

Fig. 10. Attenuation contour in decibels on x-y plane for the two-channel system with two FIR filters having 64 coefficients without constraints. (a) 400 Hz. (b) 600Hz.

In this work constraints on amplification and robust stability are added to the optimization process to prevent a high amplification and instability. Equation (27) was used in the design process. Figure 11 shows the attenuation contour over space and frequency with an amplification constraint not exceeding 20dB at the spatial axis from r=0.1m to r=0.2m for all frequencies and a constraint on robust stability with $B_1=B_2=0.3$. We can see that the attenuation area becomes smaller than that without the amplification and robust stability constraints.

In the next simulation three secondary monopoles are used to control the broadband disturbance. The attenuation contour over space and frequency for three-channel system is shown in figure 12. The secondary monopoles are located at the origin, (-0.05m, 0) and (0.05m, 0) points and the minimization region is larger than that in the two-channel system as shown in the figure. From the figure we can see that high attenuation is achieved in the desired region which is larger than that in the two secondary monopole case as shown in figure 9. It can also be seen that the shape of the high attenuation area is similar to that of the minimization region. This is because three secondary monopoles created more complicated secondary fields than those in the two secondary monopoles. Thus better performance over the minimization region was obtained as expected. High amplification also appears at high frequencies and at the region close to the secondary monopoles.
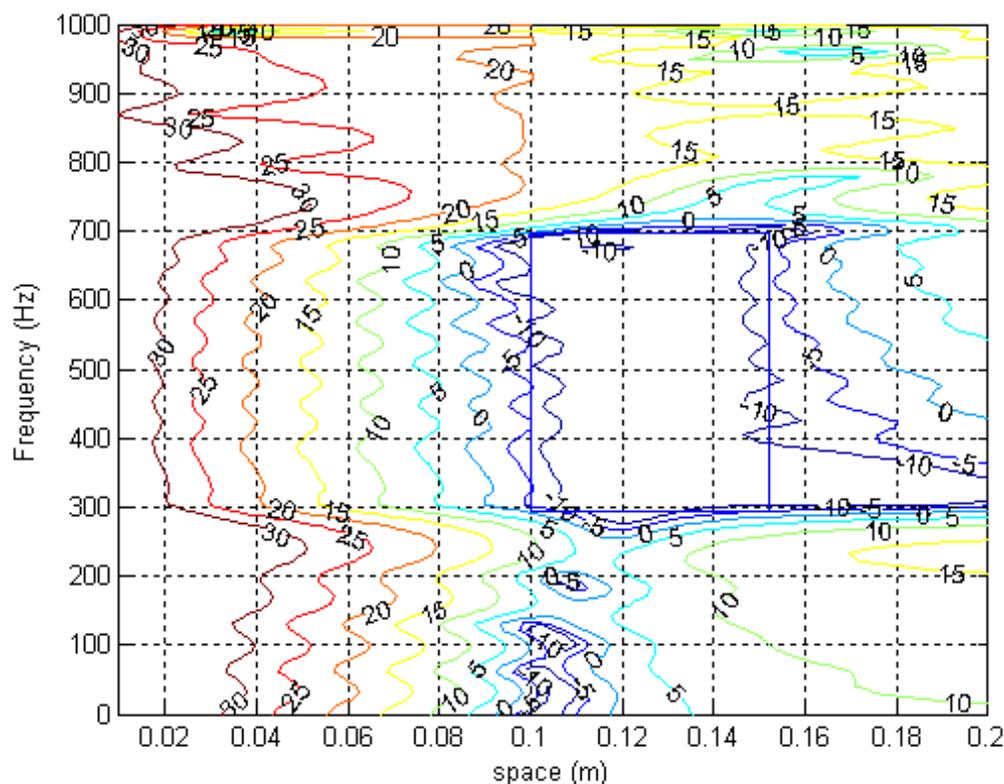

Fig. 11. Attenuation in decibels as function of space and frequency for a two-channel system with two FIR filters having 64 coefficients and with constraints on amplification not exceeding 20dB at spatial axis from r=0.1m to r=0.2m for all frequencies and constraints on robust stability with $B_1 = B_2 =0.3$.
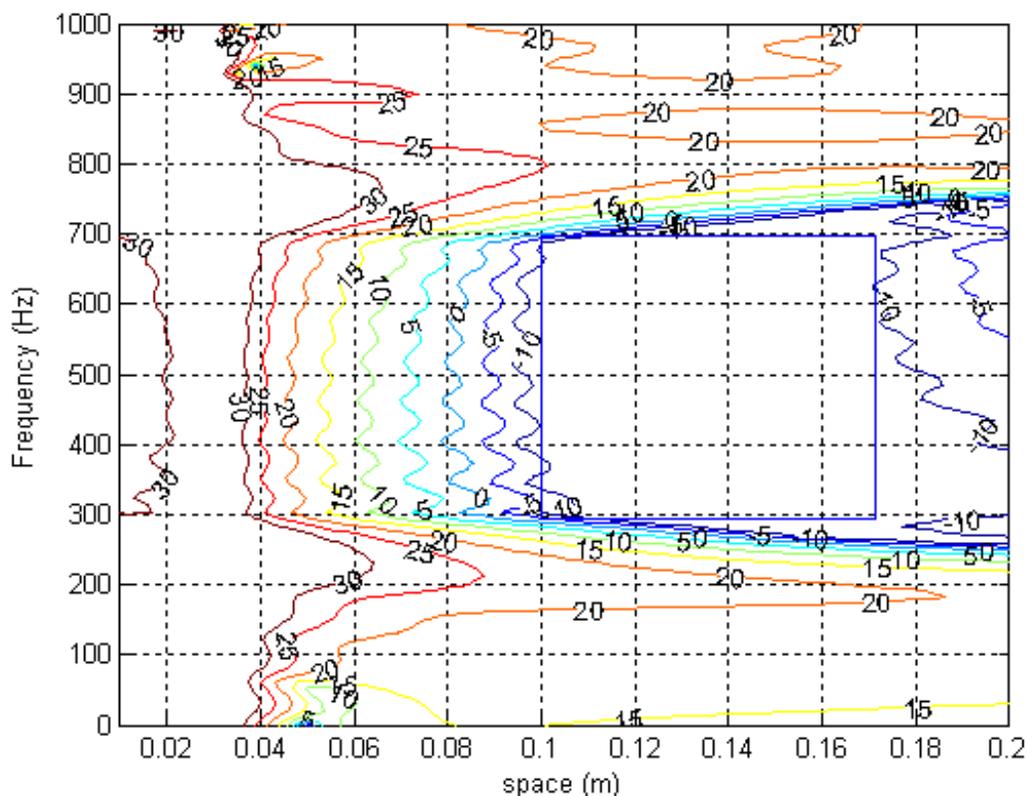
Fig. 12. Attenuation in decibels as a function of space and frequency for a three-channel system with FIR filters having 64 coefficients without constraints.

In the next simulation constraints on robust stability and amplification for the three-channel system are added in the optimization process to avoid unstable and high amplification. Figure 13 shows the attenuation contour over space and frequency for three secondary monopoles with a constraint on robust stability for $B_1=B_2=B_3=0.3$ and an amplification constraint not to exceed 20dB at the spatial axis from r=0.1m to r=0.2m for all frequencies. It can be seen that the attenuation area becomes smaller than that without constraints on robust stability and amplification for three secondary monopoles.

In the fifth example the effect of different minimization shapes on the size of the attenuation contours for three secondary monopoles has also been investigated in this study. Figures 14 (a) and (b) show the attenuation contours over space and frequency for three secondary monopoles without constraints on robust stability and amplification for different minimization shapes. It can be seen that the shape of the 10dB attenuation contour changes with the minimization shape. In figure 14 (a) the 10dB attenuation contour has a narrow shape in frequency axis and longer in space axis similar to the minimization shape. When the minimization shape changes to be narrower in space axis and longer in frequency axis, the 10dB attenuation contour tends to extend its size in the frequency axis as shown in figure 14 (b). Therefore the shape of the 10dB attenuation contour can be designed using the method presented in the work.
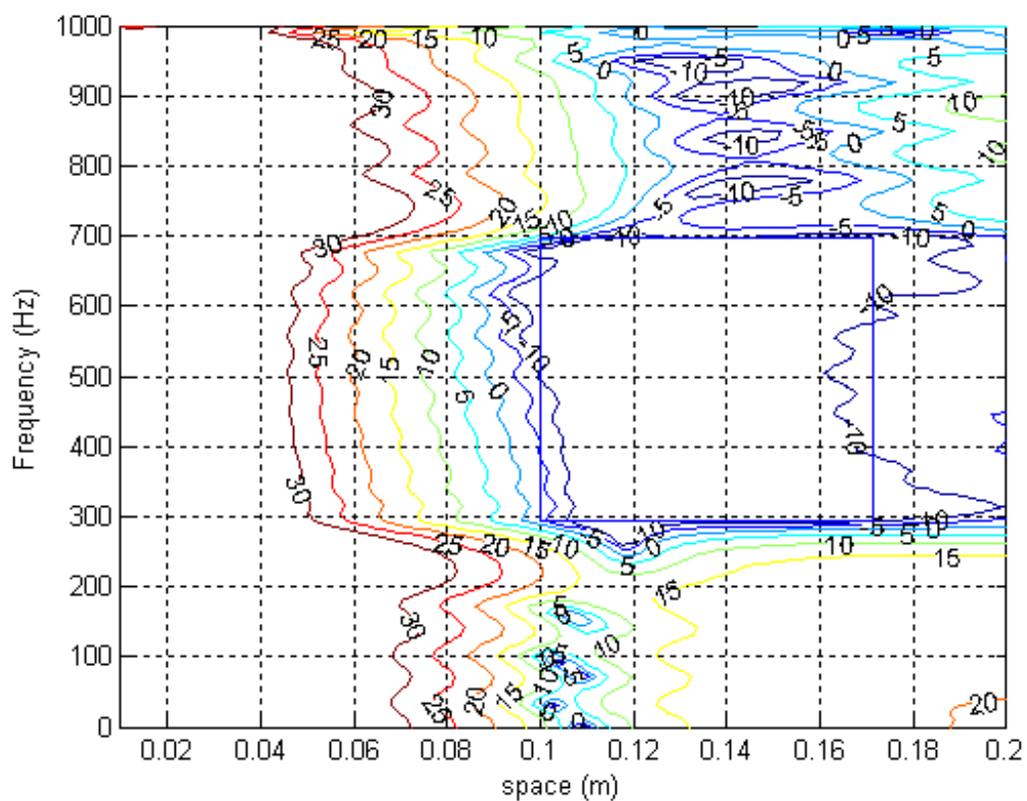
Fig. 13. Attenuation in decibels as a function of space and frequency for a three-channel system with FIR filters having 64 coefficients and constraints on robust stability for $B_1=B_2=B_3=0.3$ and amplification not to exceed 20dB at the spatial axis from r=0.1m to r=0.2m for all the frequencies.
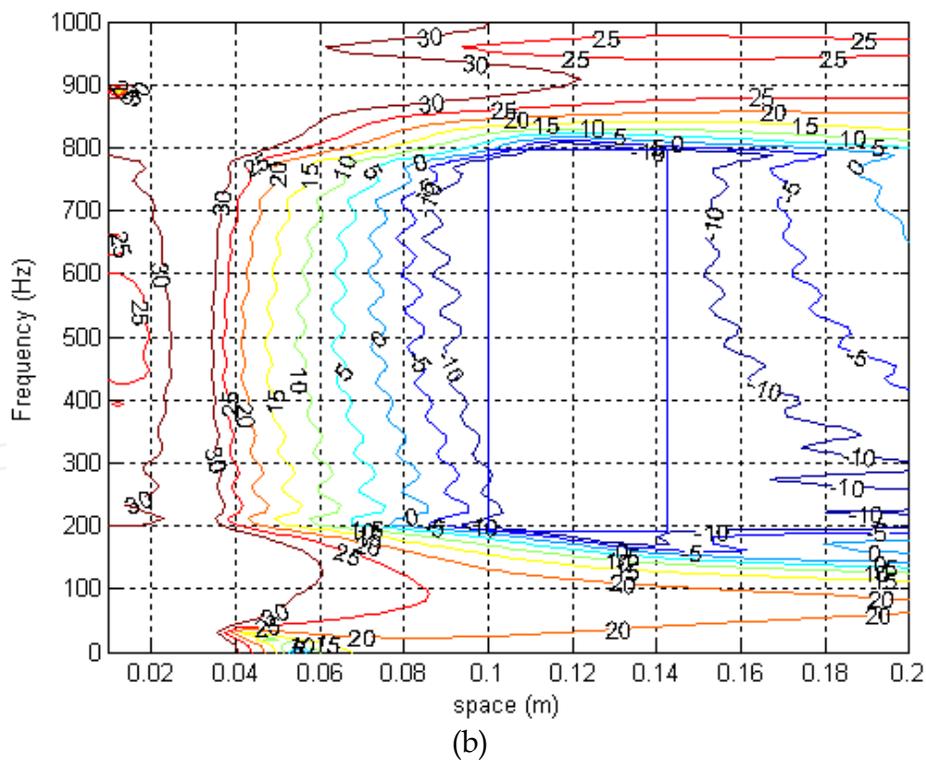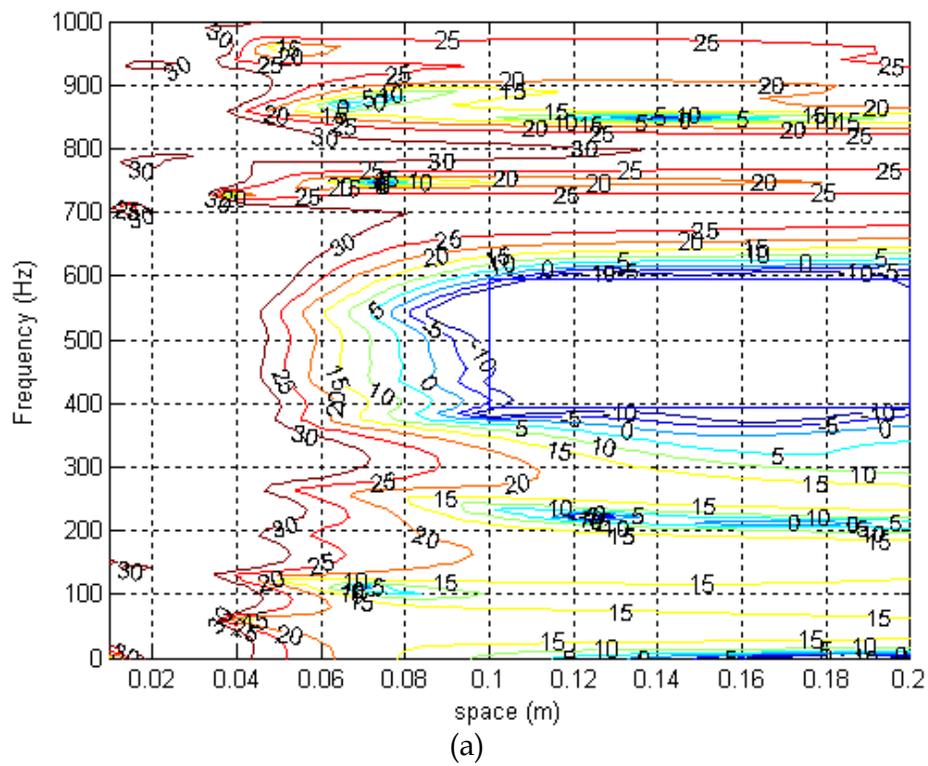
Fig. 14. Attenuation in decibels as a function of space and frequency for a three-channel system with FIR filters having 64 coefficients without constraints for the different minimization shape represented by a bold rectangular frame. (a) The rectangular frame is narrow in the frequency axis direction and longer in the space axis direction. (b) The rectangular frame is narrow in the space axis direction and longer in the frequency axis direction.

5. Experiments

In this section the experiment to validate the results of the active noise control system using ∞-norm pressure minimization has been described. The excitation frequency of 108Hz was chosen for the primary source. Figure 15 shows the experimental set-up used in the measurements. The secondary sources are two 110mm diameter loudspeakers placed separately. The grid is 30mm pitch made of 3mm diameter brass rod. The dimensions of the grid are 600×600 mm. The electret microphones of 6mm diameter are located at the corresponding nodes of the grid. The size of the room where the experiment has been performed is 10m×8m×4m and it is a normal room. The primary source was located at 4m away from the microphone grid. The primary field can be assumed to be a slightly diffuse field due to the effect of reflection.

The primary and secondary sources are connected to a dual phase oscillator that allows the amplitude and phase of the secondary sources to be adjusted. The reference signal necessary for the acquisition system to calculate the relative amplitude and phase of the complex acoustic pressure at the microphone positions is connected to a dual phase oscillator whose output can be selected with a switch that allows the signal fed to the primary source or to the secondary source to be used as a reference. An FFT analyser is connected to the reference signal to measure the frequency of excitation accurately. All the microphones are connected to an electronic multiplexer which sequentially selects three microphone signals which are filtered by the low pass filter and then acquired by the Analogue Unit Interface (AUI). The sampling frequency is 1,000 Hz and 2,000 samples are acquired for every microphone. The input signal to the AUI through channel 4 is taken as a reference to calculate the relative amplitude and phase of all the signals measured by the microphones on the grid. The calculation of the relative amplitude and phase of the pressure signals was carried out by the computer by Fourier transforming the four input signals and calculating the amplitude and phase of the microphone signals at the excitation frequency with respect to the reference signal. After a complete cycle a matrix of complex pressure values at all the grid points is therefore obtained.

At this stage, the quiet zones created by two secondary loudspeakers were investigated through experiments for one sample of primary field at 108 Hz in a room. The primary field was measured first, and the transfer functions between the secondary loudspeakers and all the microphones on the microphone grid were then measured. The primary field and transfer functions were then taken to calculate the optimal filter coefficients as in equation (26). The zone of quiet is calculated as the ratio of the total (controlled) squared pressure and the primary squared pressure. Figure 16 (a) shows the 10dB zone of quiet created by using ∞-norm pressure minimization over an area represented by the rectangular frame through computer simulations. Figure 16 (b) shows the equivalent results as in Figure 16 (a) through experiments for one sample of the primary field. It shows that the shape and size of 10dB quiet zones are similar in computer simulations and experiments. In figures 16 (a) monopole sources were used as secondary sources in simulations. In figure 16 (b), however, loudspeakers were used as secondary sources in experiments. Although monopole sources are not an accurate model of loudspeakers, it simplifies the secondary source modelling and assists comparison between simulations and experiments.
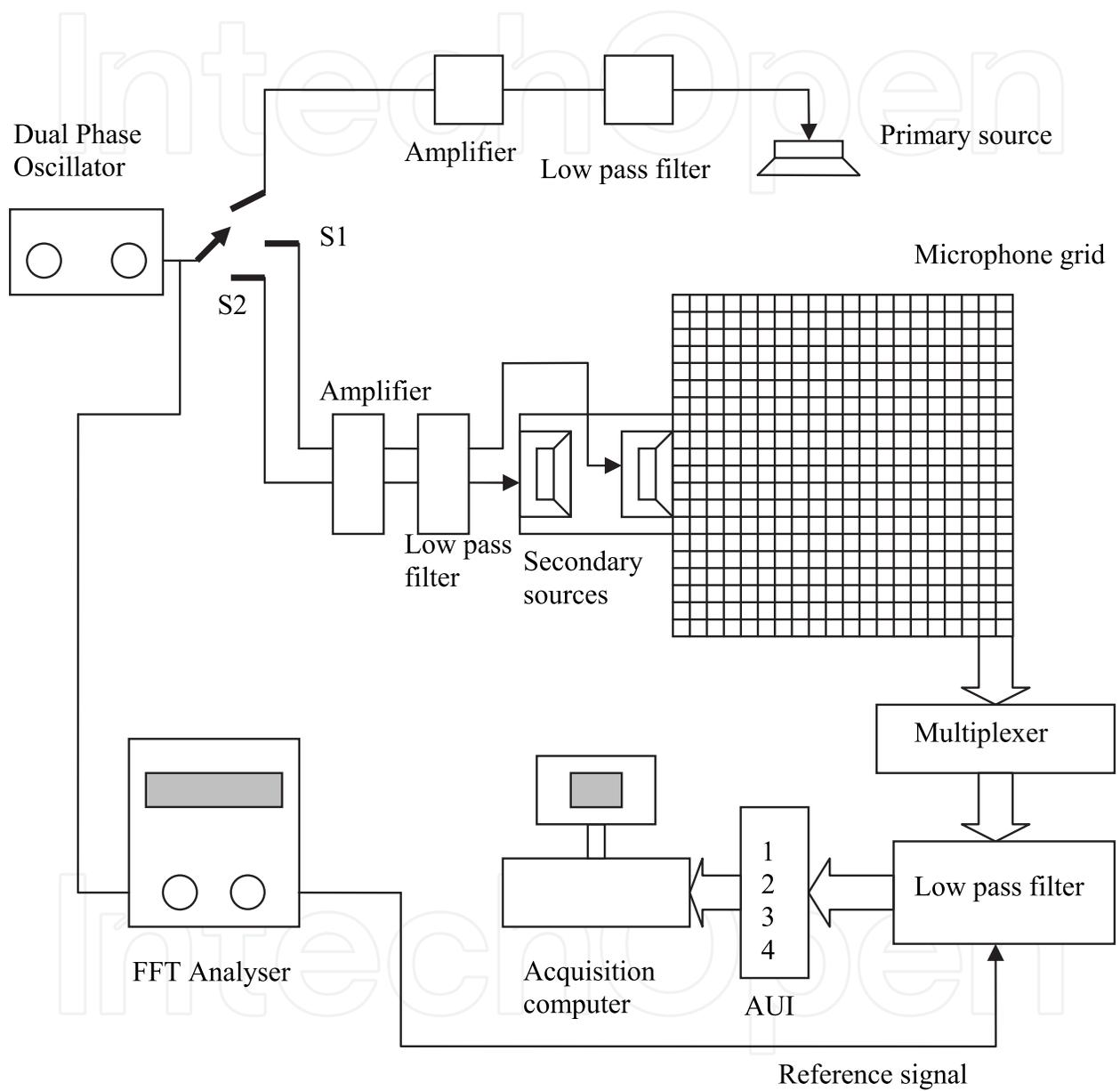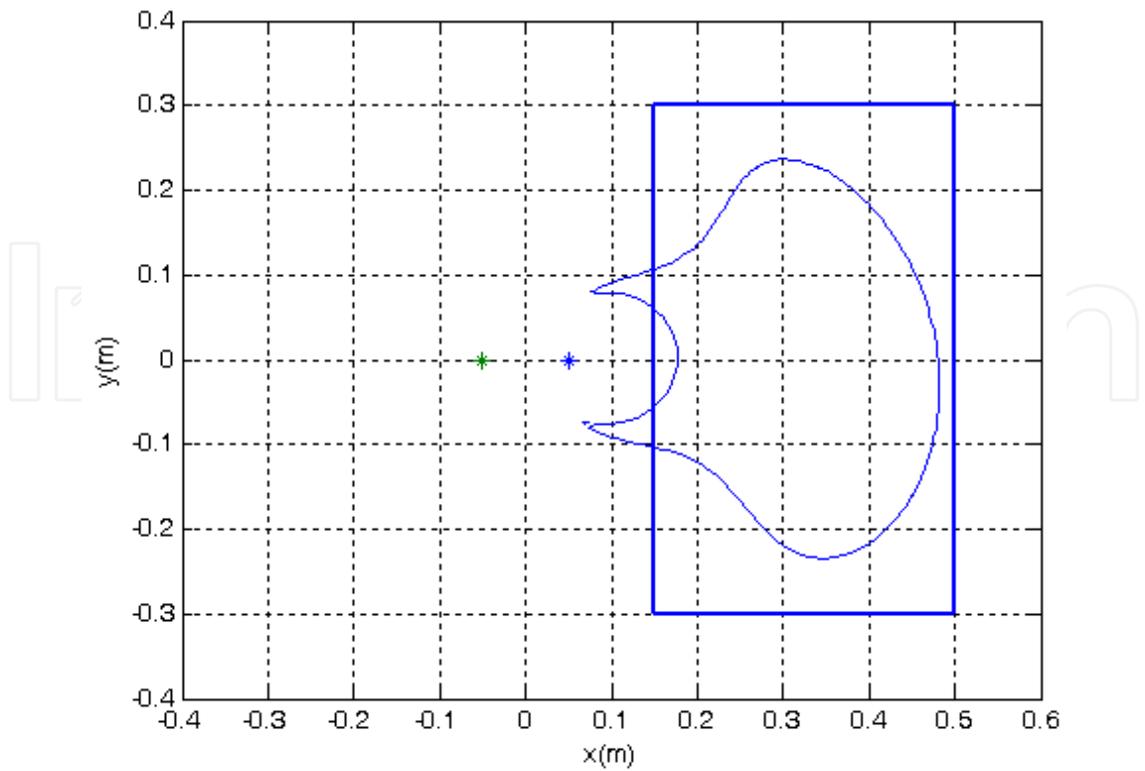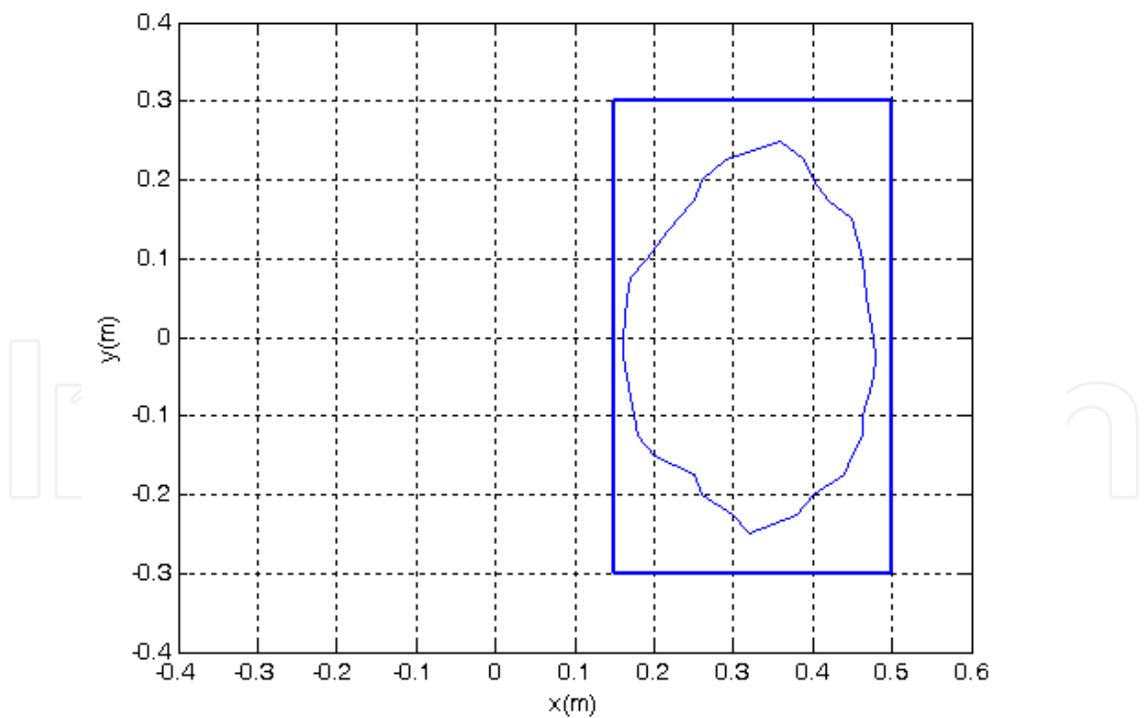
Fig. 15. Configuration of experimental set-up.

(a)

(b)

Fig. 16. The 10 dB reduction contour of the average zones of quiet created by two secondary sources located at positions (0.05, 0) and (-0.05, 0) using ∞-norm pressure minimization for 108Hz of diffuse primary fields. (a) Computer simulations. (b) Experiments.

6. Conclusions

The theory of active control for pure tone and broad-band diffuse fields using two-channel and three-channel systems has been presented and the quiet zone analysis has been investigated through computer simulations and experiments. The acoustic pressure was minimized at the specified region over space or both space and frequency. Constraints on amplification and robust stability were also included in the design process. The results showed that a good attenuation in the desired quiet zone over space or both space and frequency could be achieved using a two-channel system. However, a better performance was achieved using a three-channel system. When limits on amplification and robust stability were introduced, the performance began to degrade. It has also been shown that acoustic pressure could be minimized at a specific frequency range and at a specific location in space away from the microphone. This could be realized by virtual microphone methods. Moreover, the shape of the 10dB attenuation contour could be controlled using the proposed method.

7. Acknowledgement

8. References

C. F. Ross, C. F. (1980). Active control of sound. *PhD Thesis*, University of Cambridge.

Chun, I.; Rafaely, B. & Joseph, P. (2003). Experimental investigation of spatial correlation of broadband diffuse sound fields. *Journal of the Acoustical Society of America*, 113(4), pp. 1995-1998.

Franklin, G. F.; Powell, J. D. & Emamni Naeini, A. (1994). *Feedback control of dynamic systems*, Addison-Wesley, MA. 3rd ed.

Garcia-Bonito, J.; Elliott, S. J. & Boucher, C. C. (1997). A novel secondary source for a local active noise control system, *ACTIVE 97*, pp.405-418.

Guo, J.; Pan, J. & Bao, C. (1997). Actively created quiet zones by multiple control sources in free space. *Journal of Acoustical Society of America*, 101, pp. 1492-1501,.

Jacobsen, F. (1979). The diffuse sound field, *The Acoustics Laboratory Report* no. 27, Technical University of Denmark.

Joseph, P. (1990). Active control of high frequency enclosed sound fields, *PhD Thesis*, University of Southampton.

Miyoshi, M.: Shimizu, J. & Koizumi, N. (1994). On arrangements of noise controlled points for producing larger quiet zones with multi-point active noise control, *Inter-noise 94*, pp. 1229-1304.

Morari, M. & Zafiriou, E. (1989). *Robust process control*, Prentice-Hall, NJ.

Nelson, P. A. & Elliott, S. J. (1992). *Active Control of Sound,* Academic, London.

Rafaely, B. (2000). Spatial-temporal correlation of a diffuse sound field. *Journal of the Acoustical Society of America*. 107(6), pp. 3254-3258.

Rafaely, B. (2001). Zones of quiet in a broadband diffuse sound field. *Journal of the Acoustical Society of America*, 110(1), pp. 296-302.

Tseng, W. K.; Rafaely, B. & Elliott, S. J. (1999). 2-norm and ∞-norm pressure minimisation for local active control of sound, *ACTIVE'99*, pp.661-672.

Tseng, W. K.; Rafaely, B. & Elliott, S. J. (2000). Local active sound control using 2-norm and infinity-norm pressure minimisation. *Journal of Sound and Vibration* 234(3) pp. 427-439.

Tseng, W. K. (2009). Quiet zone design in broadband diffuse fields. *International MultiConference of Engineers and Computer Scientists*. pp. 1280-1285.

Skogestad, S. & Postlethwaite, I. (1996). *Multivariable feedback control*, John Wiley and Sons, Chichester, UK..
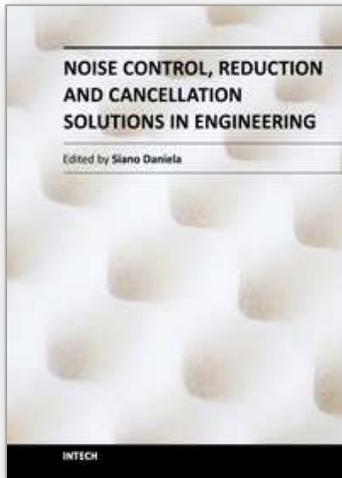
Noise Control, Reduction and Cancellation Solutions in Engineering

Edited by Dr Daniela Siano

Noise has various effects on comfort, performance, and human health. For this reason, noise control plays an increasingly central role in the development of modern industrial and engineering applications. Nowadays, the noise control problem excites and attracts the attention of a great number of scientists in different disciplines. Indeed, noise control has a wide variety of applications in manufacturing, industrial operations, and consumer products. The main purpose of this book, organized in 13 chapters, is to present a comprehensive overview of recent advances in noise control and its applications in different research fields. The authors provide a range of practical applications of current and past noise control strategies in different real engineering problems. It is well addressed to researchers and engineers who have specific knowledge in acoustic problems. I would like to thank all the authors who accepted my invitation and agreed to share their work and experiences.

How to reference

In order to correctly reference this scholarly work, feel free to copy and paste the following:

Wen-Kung Tseng (2012). Analysis of Quiet Zones in Diffuse Fields, Noise Control, Reduction and Cancellation Solutions in Engineering, Dr Daniela Siano (Ed.), ISBN: 978-953-307-918-9, InTech, Available from: http://www.intechopen.com/books/noise-control-reduction-and-cancellation-solutions-in-engineering/analysis-of-quiet-zones-in-diffuse-fields

INTECH
open science | open minds